PIPELINE COLUMN SEPARATION FLOW REGIMES

By Anton Bergant and Angus R. Simpson, Member, ASCE

ABSTRACT: A generalized set of pipeline column separation equations is presented describing all conventional types of low-pressure regions. These include water hammer zones, distributed vaporous cavitation, vapor cavities, and shocks (that eliminate distributed vaporous cavitation zones). Numerical methods for solving these equations are then considered, leading to a review of three numerical models of column separation. These include the discrete vapor cavity model, the discrete gas cavity model, and the generalized interface vaporous cavitation model. The generalized interface vaporous cavitation model enables direct tracking of actual column separation phenomena (e.g., discrete cavities, vaporous cavitation zones), and consequently, better insight into the transient event. Numerical results from the three column separation models are compared with results of measurements for a number of flow regimes initiated by a rapid closure of a downstream valve in a sloping pipeline laboratory apparatus. Finally, conclusions are drawn about the accuracy of the modeling approaches. A new classification of column separation (active or passive) is proposed based on whether the maximum pressure in a pipeline following column separation results in a short-duration pressure pulse that exceeds the magnitude of the Joukowsky pressure rise for rapid valve closure.

INTRODUCTION

Water hammer in a pipeline results in column separation when the pressure drops to the vapor pressure of the liquid. A negligible amount of free and released gas in the liquid is assumed during column separation in most industrial systems (Hansson et al. 1982; Wylie 1984). Two distinct types of column separation may occur. The first type is a localized vapour cavity with a large void fraction. A localized (discrete) vapour cavity may form at a boundary (e.g., closed valve or dead end) or at a high point along the pipeline. In addition, an intermediate cavity may form as a result of the interaction of two low-pressure waves along the pipe. The second type of column separation is distributed vaporous cavitation that may extend over long sections of the pipe. The void fraction for the mixture of the liquid and liquid-vapor bubbles in distributed vaporous cavitation is small (close to zero). This type of cavitation occurs when a rarefaction wave progressively drops the pressure in an extended region of the pipe to the liquid vapour pressure. Both the collapse of a discrete vapor cavity and the movement of the shock wave front into a distributed vaporous cavitation region condenses the vapor phase back to the liquid phase. Piping systems may therefore experience combined water hammer and column separation effects during transient events (Streeter 1983; Bergant and Simpson 1992; Wylie and Streeter 1993).

The location and intensity of column separation is influenced by several system parameters including the type of transient regime (rapid closure of the valve, pump failure, turbine load rejection), layout of the piping system (pipeline dimensions, profile, and position of the valves), and hydraulic characteristics (flow velocity, pressure head, pipe wall friction, cavitational properties of the liquid, and pipe walls). The combination of several influential parameters creates difficulties in modeling and laboratory testing of the phenomena. Due to both a lack of understanding and the occurrence of industrial accidents resulting from column separation phenomena (Bonin 1960; Parmakian 1985; Almeida 1992), designers often go to great lengths to avoid column separation in pipelines, although there are some systems in which column separation has been accepted (Provoost 1976). Engineers, however, should be able to estimate column separation effects, at least for the case of the general failure of the surge protection devices (safety analysis).

Practical implications of column separation led to intensive laboratory and field research starting at the end of 19th century (Joukowsky 1900). Column separation experiments have been performed worldwide in at least 34 experimental apparatuses (pipe diameter 0.01–0.1 m, length 10–100 m) and 7 industrial installations (up to a pipe diameter of 2.0 m, length 1,000– 10,000 m) (Bergant 1992). The experiments were mainly performed to verify numerical models. Several researchers found that for a simple reservoir-pipeline-valve system, the pressure rise after the cavity collapse at the valve may or

may not exceed the Joukowsky pressure rise and that cavities may form at the boundary or along the pipe (Martin 1983; Simpson 1986; Carmona et al. 1988; Brunone and Greco 1990; Simpson and Wylie 1991; Anderson et al. 1992; Bergant 1992). Martin (1983) defined the intensity of column separation as either limited, moderate, or severe cavitation with respect to the ‘‘number of cavitation bubbles’’ that may form in the pipeline. A similar definition has been introduced by Fan and Tijsseling (1992) for column separation induced by structural axial waves in a closed pipe. It is rather difficult to develop design criteria on the basis of cavitation intensity with the limited data available (Anderson et al. 1992; Bergant 1992).

The main objective of this paper is to develop an approach to identify column separation modes for a broad range of parameters, including initial flow velocity, static head, and pipe slope. The physical state of the liquid (either water hammer or column separation) and the maximum pipeline pressure (design criteria) are the two governing parameters identifying the modes of behavior (Bergant 1992). A combined experimental-theoretical analysis of column separation flow regimes is performed for the rapid closure of a downstream end valve in the experimental apparatus (Bergant and Simpson 1995). In addition, a generalized set of pipeline column separation equations describing the particular state of the liquid is presented with analytical and numerical methods for solving these equations. A column separation algorithm for various types of pipe configurations and various cases of flow interactions is developed with the aid of existing numerical tools. The discrete vapor cavity model (DVCM), the discrete gas cavity model (DGCM), and the generalized interface vaporous cavitation model (GIVCM) are compared with measured results.

PIPELINE COLUMN SEPARATION EQUATIONS

Column separation in pipelines may be described by a set of 1D equations representing a particular physical state of the fluid. These equations include water hammer equations for the liquid phase, two-phase flow equations for a distributed vaporous cavitation region, shock equations for condensation of liquid-vapor mixture back to the liquid, and equations for a discrete vapor cavity separating a liquid and/or a vaporous cavitation region.

Water Hammer Equations

Water hammer equations for transient liquid flow are valid only when the pressure is above the liquid vapor pressure and include the continuity equation and equation of motion (Wylie and Streeter 1993)

$$\frac{\delta H}{\delta t} + V\frac{\delta H}{\delta x} - V\sin\theta + \frac{a^2}{g}\frac{\delta V}{\delta x} = 0 \tag{1}$$

$$g\frac{\delta H}{\delta x} + \frac{\delta V}{\delta t} + V\frac{\delta V}{\delta x} + \frac{fV|V|}{2D} = 0 \tag{2}$$

in which H = piezometric head (hydraulic grade line); t = time; V = flow velocity; x = distance; θ = pipe slope; a = water hammer wave speed; g = gravitational acceleration; f = Darcy-Weisbach friction factor; and D = pipe diameter.

Two-Phase Flow Equations for Distributed Vaporous Cavitation Region

A distributed vaporous cavitation region (zone) is described by the two-phase flow equations for a homogeneous mixture of liquid and liquid-vapor bubbles (liquid-vapor mixture). Pressure waves do not propagate through an established distributed vaporous cavitation zone because it is at an assumed constant vapor pressure. Two-phase flow equations are the continuity equation and equation of motion (Bergant and Simpson 1992; Wylie and Streeter 1993)

$$\frac{\delta \alpha_v}{\delta t} + V_m\frac{\delta \alpha_v}{\delta x} - \frac{\delta V_m}{\delta x} = 0 \tag{3}$$

$$\frac{\delta V_m}{\delta t} + V_m\frac{\delta \alpha_v}{\delta x} + g\sin\theta + \frac{fV_m|V_m|}{2D} = 0 \tag{4}$$

in which α_v = void fraction of vapor; and V_m = liquid-vapor mixture velocity.

Shock Equations for Condensation of Liquid-Vapor Mixture Back to Liquid

A distributed vaporous cavitation region expands by propagating into a water hammer region. Eventually, the distributed vaporous cavitation region stops expanding and the boundary separating the water hammer and vaporous cavitation regions commences to move back into the cavitation region. The progression of the liquid into the liquid-vapor mixture or the collapse of a discrete vapor cavity separating the mixture zone(s) (end or intermediate cavity) condenses the liquid-vapor mixture back to liquid. The liquid is then compressed to a pressure that is greater than the liquid-vapor pressure. The movement of the interface (shock wave front) separating the one-phase fluid (liquid) and the two-phase fluid (liquid-vapor mixture) is described by the shock equations. The shock equations developed for the control volume shown in Fig. 1 are the continuity equation and equation of motion (Bergant and Simpson 1992)

$$a_s\left[\frac{g}{a^2}(H_s - H_{sv}) + \alpha_v\right] - (V - V_m) = 0 \tag{5}$$

$$g(H_s - H_{sv}) + (V - V_m)(V - V_m - a_s) = 0 \tag{6}$$

in which a_s = shock wave speed; H_s = piezometric head on the water hammer side of the shock wave front; and H_{sv} = piezometric head on the distributed vaporous cavitation side of the shock wave front. The shock wave equations are coupled with water hammer and liquid-vapor mixture equations.

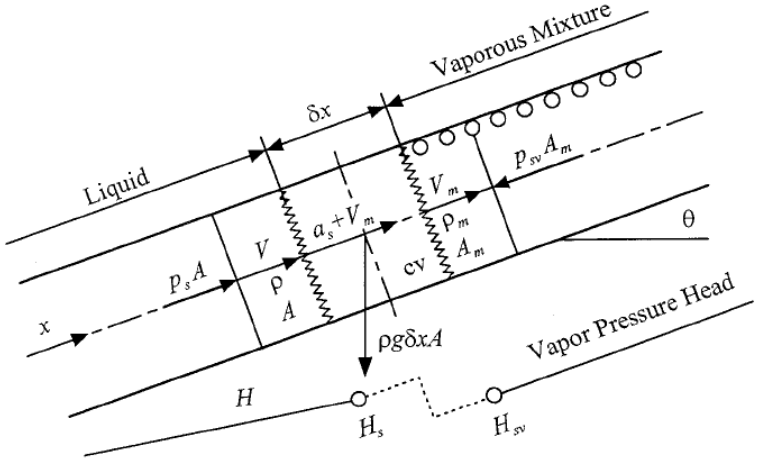

Fig 1: Control Volume for Shock Equations

Equations for a Discrete Vapor Cavity

The growth and subsequent decay of a localized (discrete) vapor cavity is defined by the following continuity equation (Streeter 1969):

$$\forall_{vc} = \int_{t_{in}}^{t} A(V - V_u)dt \tag{7}$$

in which $\forall_{vc}$ = discrete vapor cavity volume; t_{in} = time of inception of the discrete vapor cavity; A = pipe area; V = outflow velocity at the downstream side of the vapor cavity; and V_u = inflow velocity at the upstream side of the vapour cavity. The continuity equation is coupled to the water hammer and/or two-phase liquid-vapor mixture flow equations to account for flow velocities.

ANALYTICAL AND NUMERICAL TOOLS

The governing equations are solved separately for water hammer regions [(1) and (2)], distributed vaporous cavitation zones [(3) and (4)], the movement of the shock wave fronts [(5) and (6)], and discrete vapor cavities [(7)]. A simple form of the method of characteristics water hammer

compatibility equations $C1$ and $C2$ is used in most column separation models (Wylie and Streeter 1993; Simpson and Bergant 1994)

$$C^+ \quad for \quad \Delta x/\Delta t = a: \quad H_j = C_P - B_P Q_{uj} \tag{8}$$

$$C^- \quad for \quad \Delta x/\Delta t = -a: \quad H_j = C_M + B_M Q_j \tag{9}$$

in which Δx = reach length; Δt = time step; B_M, B_P, C_M, and C_P = known constants in water hammer compatibility equations; Q_{uj} = discharge at the upstream side of the computational section j; and Q_j = discharge at the downstream side of the section. Incorporating discrete vapor cavities into the water hammer solution methods leads to the DVCM (Streeter 1969; Wylie and Streeter 1993; Simpson and Bergant 1994). Coupling the complete set of column separation methods gives the interface vaporous cavitation (consolidation) model—GIVCM (Streeter 1983; Bergant and Simpson 1992).

Analytical and Numerical Integration for Two-Phase Flow Liquid-Vapor Mixture Equations
Eqs. (3) and (4) can be solved analytically (Streeter 1983). An approach to the solution of the two equations for an upward sloping pipe by Simpson (1986), and then extended to a downward sloping and horizontal pipe by Bergant (1992), is presented. Introducing the total derivative, the velocity of liquid- vapor mixture V_m is first calculated from (4) by analytical integration, then the void fraction α_v is estimated by numerical integration of (3).

The solution of (4) for V_m depends on the pipe slope (upward, downward, or horizontal) and the inception velocity of the liquid-vapor mixture V_{mi} at time of cavitation inception t_i at a distance x along the pipeline, at which the pressure drops to the liquid-vapor pressure. The inception velocity V_{mi} is calculated from (8) or (9) within the method of characteristics numerical grid with the pressure set to the vapor pressure. The results of integration for V_m are as follows (Bergant 1992).

Sloping Pipe with $\theta V_{mi} > 0$
There are two situations for this case: (1) θ is positive and V_{mi} is positive; or (2) θ is negative and V_{mi} is negative.

Before flow reversal:

$$V_m = V_{mt} \tan\left(\tan^{-1}\left(\frac{V_{mi}}{V_{mt}}\right) - \text{sign}(\theta)\frac{fV_{mt}}{2D}(t - t_i)\right) \tag{10}$$

in which $V_{mt} = (2gD|\sin\theta|/f)^{1/2}$ = terminal velocity of the liquid-vapor mixture in the sloping pipe and sign(θ) = (+1 for θ > 0 or -1 for θ < 0).

After flow reversal:

$$V_m = V_{mt}\frac{e^{-\text{sign}(\theta)fV_{mt}(t-t_r)/D} - 1}{e^{-\text{sign}(\theta)fV_{mt}(t-t_r)/D} + 1} \tag{11}$$

in which the time of flow reversal t_r is

$$t_r = t_i + \text{sign}(\theta)\frac{2D}{fV_{mt}}\tan^{-1}\left(\frac{V_{mi}}{V_{mt}}\right) \tag{12}$$

Sloping Pipe with $uVmi < 0$

There are two situations for this case: (1) θ is positive and V_{mi} is negative; or (2) θ is negative and V_{mi} is positive

$$V_m = V_{mt}\frac{V_{mi}-V_{mt}+(V_{mt}+V_{mi})e^{-\text{sign}(\theta)fV_{mt}(t-t_r)/D}}{V_{mt}-V_{mi}+(V_{mt}+V_{mi})e^{-\text{sign}(\theta)fV_{mt}(t-t_r)/D}} \quad (13)$$

Horizontal Pipe

$$V_m = \frac{2DV_{mi}}{2D+\text{sign}(V_{mt})fV_{mi}(t-t_i)} \quad (14)$$

in which sign(V_{mi}) = (+1 for $V_{mi} > 0$ or -1 for $V_{mi} < 0$). Numerical integration of (3) at time t for the void fraction α_v over a time step Δt, assuming a weighting factor ψ in time direction (Wylie 1984), gives

$$(\alpha_v)_{k,t} = (\alpha_v)_{k,t-\Delta t} + \{\psi[(V_m)_{j+1,t} - (V_m)_{j,t}] + (1-\psi)[(V_m)_{j+1,t-\Delta t} - (V_m)_{j,t-\Delta t}]\}\Delta t/\Delta x \quad (15)$$

in which j = number of the upstream node; and $j + 1$ = number of the downstream node for the computational reach k of length Δx ($\Delta x = a\Delta t$).

Newton-Raphson Method for Coupled Shock Equations

Eqs. (5) and (6) form a system of algebraic equations describing the movement of the shock wave front into the liquidvapor mixture. The shock equations are coupled with (8) or (9), depending on the direction of travel of the interface, the kinematic equation for the length of the front movement, and the equation of motion for the liquid plug condensed over a part of the reach. Let L be the distance to the shock interface measured from the nearest computational section (through the liquid plug). The kinematic equation for the position of the shock interface as it moves from $L_{t-\Delta t}$ to L_t during the time step Δt is

$$L_t = L_{t-\Delta t} + |a_s + V_m|\Delta t \quad (16)$$

The equation of motion written for the liquid plug of length L_t is

$$\text{sign}(a_s)(H_j - H_s) - \frac{fL_t}{2gDA^2}Q_j|Q_{j,t-\Delta t}| - \frac{L}{gA\Delta t}(Q_j - Q_{j,t-\Delta t}) = 0 \quad (17)$$

in which sign(a_s) = (+1 for $a_s > 0$ or -1 for $a_s < 0$); and H_j = piezometric head at the upstream side of the liquid plug at computational section j. Note that $Q_{uj} = Q_j$ at the upstream end of the liquid plug.

The unknowns in the above system are H_j, H_s at the water hammer side of the interface, and Q_j, as, and L_t. V_m is calculated directly from one of (10)–(14) and α_v from (15). This system of nonlinear equations is solved by the Newton-Raphson method (Carnahan et al. 1969). The development of shock equations for the collapse of an intermediate cavity located between two distributed vaporous cavitation regions and for the end boundary conditions (e.g., reservoir, valve) is described in the literature [e.g., Simpson (1986), Bergant (1992), and Bergant and Simpson (1992)].

Numerical Integration of Discrete Vapor Cavity Continuity Equation

The volume of a discrete cavity given by (7) is solved by numerical integration using a weighting factor c in the time direction within the staggered grid of the method of characteristics (Wylie 1984; Simpson and Bergant 1994)

$$(\forall_{vc})_{j,t} = (\forall_{vc})_{j,t-2\Delta t} + [(1-\psi)(Q_{j,t-2\Delta t} - Q_{uj,t-2\Delta t}) + \psi(Q_{j,t} - Q_{uj,t})]2\Delta t \quad (18)$$

The discharges on either side of the cavity are given by (8) and (9) (with the pressure set to the vapor pressure) as the two adjacent sections are in the water hammer region. One of (10)–(14) is used when a reach adjacent to the discrete vapour cavity becomes a vaporous cavitation region. The cavity collapse (that occurs when the cumulative cavity volume becomes less than zero) generates water hammer and/or shock waves.

DVCM

The DVCM for simulating pipeline column separation is used in most engineering transient simulation software packages (Safwat et al. 1986). The model allows vapor cavities to form at any computational section in the method of characteristics when the pressure at the section is calculated to drop to or below the liquid vapor pressure (Streeter 1969; Wylie and Streeter 1993). A liquid phase with a constant wave speed a between the computational sections is assumed. It is recommended that the staggered grid should be used in preference to the normal rectangular grid (Simpson and Bergant 1994).

The DVCM may generate unrealistic pressure spikes associated with multicavity collapse. The model approximately represents the real physical situation when a distributed vaporous cavitation zone is established and then condensed back to the liquid phase (often with a highly variable shock wave speed). The DVCM gives reasonably accurate results when the number of reaches is restricted (the ratio of maximum cavity size to reach volume should be below 10%) and sensitivity analysis to input parameters is performed (Simpson and Bergant 1994).

A number of variations of the standard DVCM have been introduced (Safwat and van der Polder 1973; Kot and Youngdahl 1978; Provoost and Wylie 1981; Miwa et al. 1990) to improve the performance of the DVCM. The DGCM developed by Provoost and Wylie (1981) performs consistently over a broad range of parameters when a small gas void fraction at the computational section ($\alpha_g \leq 10^{-7}$) is selected (Barbero and Ciaponi 1992; Bergant 1992; Simpson and Bergant 1994). The growth and collapse of the gas cavity is calculated from (8), (9), and (18) and the ideal gas equation (Wylie and Streeter 1993).

GIVCM

An interface vaporous cavitation (consolidation) model couples the complete set of analytical and numerical methods for solving pipeline column separation equations into a single algorithm (Streeter 1983; Simpson 1986; Bergant 1992; Bergant and Simpson 1992). The GIVCM for a number of pipeline configurations (sloping and horizontal pipe) and various interactions between water hammer regions, distributed vaporous cavitation zones, intermediate cavities (along the pipeline), and cavities at boundaries (valve, high point) has been developed (Bergant 1992; Bergant and Simpson 1992).

The standard DVCM algorithm allows cavities to form at computational sections in the staggered grid of the method of characteristics (Wylie and Streeter 1993; Simpson and Bergant 1994) and has been used as a basis for the development of the GIVCM. The incorporation of the distributed vaporous cavitation zones, shock waves, and various types of discrete cavities are important features in modifying the standard DVCM.

The GIVCM algorithm maintains the same basic structure as the DVCM. Transient analysis is first performed at interior and then at boundary computational sections. A loop for the shock treatment at appropriate computational sections is added to the basic DVCM loop in which a module for combined discrete vapor cavity and distributed vaporous cavitation computation is incorporated. The algorithm is supported by flags to control the correct physical behavior of various phase interactions and to identify possible new interactions. Each physical flow condition at a computational section j (either liquid, discrete vapor cavity, vaporous mixture, or shock wave front) is compared with flow conditions within the upstream and downstream computational pipe reaches and at computational sections $j - 1$ and $j + 1$.

The GIVCM performs consistently over a broad range of parameters (Bergant 1992). More accurate treatment of distributed vaporous cavitation zones, shock waves, and various types of discrete cavities contribute to improved performance of the pipe column separation model. The drawback of the model in comparison with the discrete cavity models is the complex structure of the algorithm and longer computational time for the run (CPU). Complexity of flow conditions (combinations of various regions) and pipeline configurations govern the CPU usage. Details of CPU run times for each of the models are given in the results section of this paper.

EXPERIMENTAL APPARATUS

A flexible experimental apparatus for investigating water hammer and column separation events in pipelines has been designed and constructed (Bergant 1992; Bergant and Simpson 1995). The apparatus shown in Fig. 2 is composed of a copper straight 37.23 m ($U_x = \pm 0.01$ m) long sloping pipeline of 22.1 mm ($U_x = \pm 0.1$ mm) internal diameter and 1.6 mm ($U_x = \pm 0.05$ mm) wall thickness connecting two pressurized tanks (where U_x = uncertainty in a measurement expressed as a rootsum-square combination of bias and precision errors) [see Coleman and Steele (1989)]. The pipe slope has a constant value of $\theta = 3.2°$ or 1 (vertical) to 18.3 (horizontal). The design pressure of the pipeline is 5,000 kPa. Demineralized water was used as the fluid.

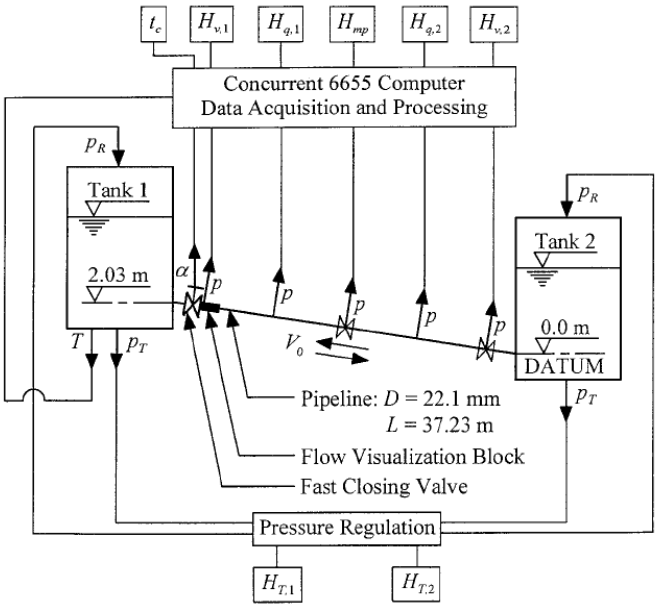

Fig 2: Experimental Apparatus Layout

A pressure control system for maintaining a specified pressure in each of the tanks enables the simulation of transients in either an upward or a downward sloping pipeline. The pressure in both tanks may be regulated from 20 to 620 kPa to simulate low-head or medium-head hydraulic systems. However, the net water volume in both tanks and the capacity of the air compressor limit the maximum steady-state velocity to 1.5 m/s and maximum operating pressure (pressure head) in each tank to 400 kPa (40 m).

Water hammer events including column separation in the experimental apparatus are initiated by rapid closure of a ball valve. The valve can be located at either end of the pipeline adjacent to either tank or at the midpoint of the pipeline; thus, simulation of various types of pipe configurations can be performed. The valve is closed by a torsional spring actuator or it is closed manually by hand. The actuator provides a constant and repeatable valve closure time. The spring is pretensioned to vary the closure time from 5 to 10 ms. The effective valve closure (actual flow decrease) time is about 40% of the total valve closure time, i.e., from 2 to 4 ms.

Pressure transducers are located at five equidistant points along the pipeline, as close as possible to the endpoints. The piezoelectric pressure transducers (Kistler 610 B) are positioned at the endpoints and at the midpoint, whereas the straingauge transducers (Druck PDCR 810) are installed at all five points. In addition, the water temperature in Tank 1 is continuously monitored and the valve position during closure is measured precisely using optical sensors. Data acquisition and processing were performed with a Concurrent 6655 real-time UNIX data acquisition computer. A flow visualization block of a polycarbonate (Lexan) of 150 mm length and 22.1 mm internal diameter is also incorporated into the pipeline system. A high-speed video was used to photograph the evolution and collapse of vapor cavities at the valve (Bergant and Simpson 1996).

After an initial steady state is established, a transient event is initiated by a rapid valve closure. The measured steady-state quantities include the pressure in each tank ($U_x = \pm 0.3\%$), barometric pressure ($U_x = \pm 0.1$ kPa), and ambient temperature ($U_x = \pm 0.5°C$). The time-dependent quantities are pressures at five equidistant points along the pipeline ($U_x = \pm 0.7\%$ for the piezoelectric pressure transducers, $U_x = \pm 0.3\%$ for the straingauge pressure transducers), valve closure time ($U_x = \pm 0.0001$ s), and water temperature ($U_x = \pm 0.5°C$). The initial steadystate velocity in a pipeline is measured indirectly by the volumetric method ($U_x = \pm 1\%$) and the water hammer method ($U_x = \pm 0.7\%$). The flow velocity determined by the volumetric method is proportional to the change in water level over a period of time in either of the upstream or downstream tanks. The water hammer method pipe flow velocity is computed from the Joukowsky pressure head rise or pressure head drop (for water hammer case only) resulting from a fast closure of the valve. The wave-propagation velocity ($Ux = \pm 0.1\%$) is obtained from the measured time for a water hammer wave to travel between the closed valve and the quarter point nearest the valve.

NUMERICAL AND EXPERIMENTAL FINDINGS

Numerical and experimental analysis of the influence of a number of quantities on column separation events in the experimental apparatus (Fig. 2) is presented including initial flow velocity, static head, and pipe slope. Numerical results from the DVCM, DGCM, and GIVCM are compared with results of measurements. Computational and experimental runs were performed for a rapid closure of the valve positioned at the downstream end of the sloping pipe (upward, downward; Fig. 2). The valve closure time for all runs was identical, $t_c = 0.009$ s (the effective time of closure is 0.004 s), which is significantly shorter than the water hammer wave reflection time of $2L/a = 2 \times 37.23/1{,}319 = 0.056$ s ($a = 1{,}319$ m/s is the measured wave speed). The sampling frequency for each dynamic measured quantity in the apparatus was $f_s = 5{,}000$ Hz. The results of similar initial conditions showed a high degree of repeatability of the magnitude and timing of main pressure pulses, whereas some high-frequency spikes did not exhibit similar repeatability (Bergant and Simpson 1995; Simpson and Bergant 1996). Pressures measured at the equidistant points along the pipe are compared with computational results as piezometric heads (or heads) with a datum level at the top of the pipe at Tank 2 (elevation 0.0 m in Fig. 2).

The rapid valve closure begins at time $t = 0.0$ s. The numerical parameters selected in each of the three column separation models and for each computational run are the number of reaches $N = 16$, a weighting factor of $\psi = 1.0$; and in addition, a gas void fraction $\alpha_g = 10^{-7}$ was used in DGCM (Wylie 1984). The number of reaches was restricted to ensure reasonably accurate DVCM predictions (Anderson and Arfaie 1992; Simpson and Bergant 1994). A steady-state friction model was used in all computational runs (Bergant and Simpson 1994).

The temporal behavior of measured and computed piezometric heads at selected sections along the experimental pipe is presented for five distinct runs to present the influence of the initial velocity, static pressure head in each tank, and pipe slope on a column separation event. The strengths and weaknesses of the DVCM, DGCM, and GIVCM are assessed. In addition, a global comparison is made for a total of 60 runs for two different static tank heads (measured at the valve) for both an upward and downward sloping pipe to verify the robustness of the models for a broad range of parameters.

Comparison of Numerical and Experimental Runs for Different Initial Flow Velocities

The results for two distinct different flow velocity cases in an upward sloping pipe (Fig. 2) $V_0 = (0.30; 1.40)$ m/s for a constant upstream end reservoir head (Tank 2) $H_{T,2} = 22.0$ m are presented. The low-velocity case represents a column separation event with a maximum pressure larger than the Joukowsky valve closure pressure; the high-velocity column separation case generates a maximum pressure lower than the valve closure pressure.

Numerical model and measured piezometric heads at the valve $H_{v,1}$, at two quarter points $H_{q,1}$ and $H_{q,2}$, and at the midpoint H_{mp} (Fig. 2) are presented for the low-velocity case $V_0 = 0.30$ m/s. The head adjacent to the upstream end reservoir ($H_{v,2}$ for the upward sloping pipe in Fig. 2) is the reservoir head.

A comparison of experimental results and results for DVCM, DGCM, and GIVCM is shown in Figs. 3–5, respectively.

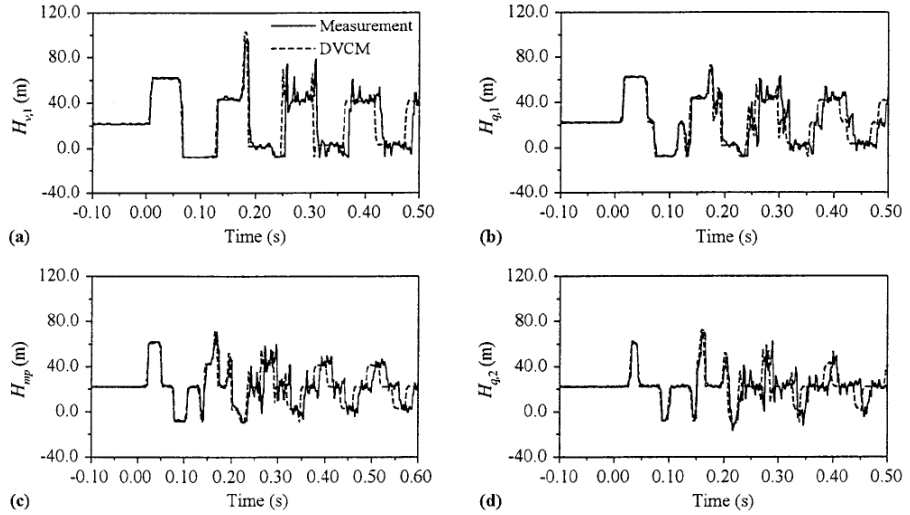

Fig 3: Comparison of Heads along Upward Sloping Pipe for DVCM and Measured Results; V_0 = 0.30 m/s

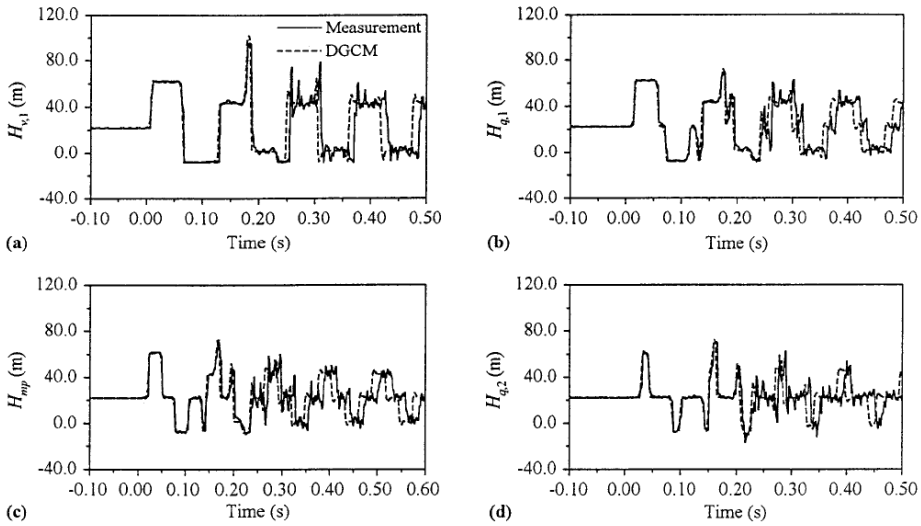

Fig 4: Comparison of Heads along Upward Sloping Pipe for DGCM and Measured Results; V_0 = 0.30 m/s

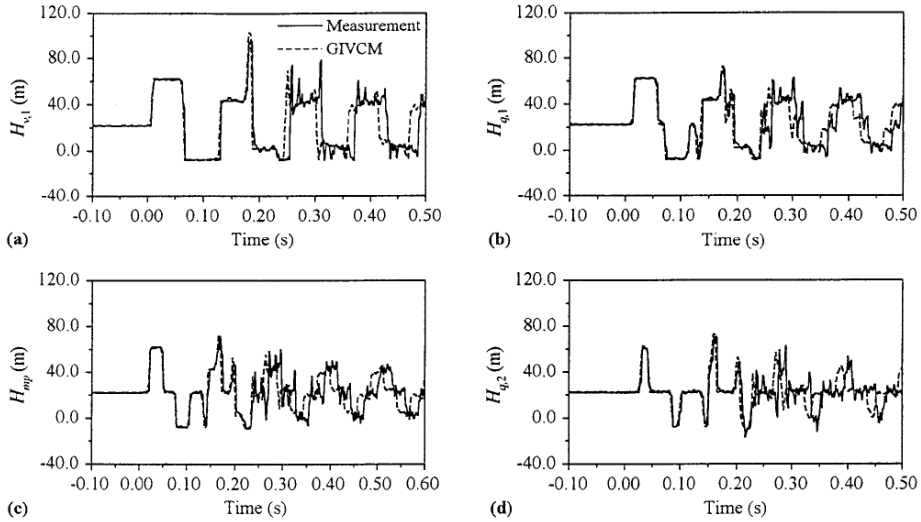

Fig 5: Comparison of Heads along Upward Sloping Pipe for GIVCM and Measured Results; V_0 =0.30 m/s

The valve closure for V_0 = 0.30 m/s generates water hammer ($H_{v,1}$ = 62.5 m) and subsequent column separation at the valve in a time of 0.0662 s. Pressure at the three locations along the pipe is above the vapor pressure [flat hydraulic grade line (HGL)]. The cavity at the valve collapsed in a time of 0.1298 s. The head generated by the cavity collapse is less than the water hammer head. The maximum measured head $H_{\max;v,1}$ = 95.6 m occurs in a time of 0.1842 s as a narrow short-duration pressure pulse (Simpson 1986), resulting from the superposition of the collapsed cavity head and the reservoir wave head doubled by the wave reflection from the closed valve. The magnitude of the short-duration pressure pulse predicted by DVCM, DGCM, and GIVCM $H_{\max;v,1}$ = (102.4; 101.9; and 102.5) m is higher when compared with the experimental result. There is good agreement between the results for the maximum peak at two quarter points and at the midpoint. The duration of the first cavity at the valve $t_{\forall max;v,1}$ = [measurement: 0.0636 s (2.253L/a); DVCM, DGCM, GIVCM: 0.0635 (2.253L/a)] s is controlled by the amount of the water hammer head decrease to the vapor pressure head when the wave is reflected off the closed valve at 2L/a (76% of the Joukowsky head $\Delta H = aV_0/g$ = 1319 × 0.30/9.81 = 40.3 m) and flow conditions in the pipeline (head in the upstream end tank, pipe friction, and pipe slope). The timing match between the DVCM, DGCM, and GIVCM and the experimental results is good until 0.22 s, when the pressure at the three sections along the pipeline drops to the vapor pressure for the first and the last time during a transient event. The measured piezometric head traces along the pipe ($H_{q,1}$, H_{mp}, and $H_{q,2}$) indicate the formation of an intermediate cavity between the reservoir (Tank 2) and the upstream end one-quarter point ($H_{q,2}$) followed by propagation of a distributed vaporous cavitation region from the cavity toward the valve passing $H_{q,2}$ in a time of 0.216 s, H_{mp} of 0.223 s, and $H_{q,1}$ of 0.230 s. Pressure traces at the two quarter points and the midpoint show a similar behavior. Pressure measurements at three different locations along the pipe enables accurate tracing of intermediate cavities and propagation of a vaporous cavitation zone formed along the pipeline. All three numerical models predict the formation of an intermediate cavity 4.65 m away from the upstream end reservoir at 0.212 s, resulting in propagation of a negative wave toward the reservoir passing $H_{q,2}$ at 0.215 s, H_{mp} at 0.222 s, and $H_{q,1}$ at 0.229 s. The differences between the numerical results and the results of measurements increase after this time. All three models predict the maximum volume of the intermediate cavity of ~0.05% of reach volume and the time of cavity collapse at 0.222 s. The collapse of the intermediate cavity is indicated as a high-frequency, low-amplitude pressure head spike superimposed with the reservoir wave traveling toward the valve, and is subsequently attenuated in succeeding pressure rise traces. The major difference between the three models is in the physical description of a distributed vaporous cavitation zone that expands from the intermediate cavity toward the valve and is subsequently condensed back to the liquid phase. Expansion and compression of the liquid-vapor mixture in DVCM and DGCM is described by discrete cavities lumped at computational sections. The distributed vaporous region in GIVCM is described by two-phase flow equations; the mixture is condensed back to the liquid phase by an incoming shock wave front. Experimental results exhibit an additional low-amplitude pressure spike that was not predicted by the three models. The increased differences in timing between the computed and experimental results for the third and fourth major pressure pulse are likely due to unsteady friction effects (pressure above the vapor pressure). The ratio of the CPU user time for DVCM:DGCM:GIVCM is 1:1.6:2.4.

The maximum head at the valve for a velocity of 1.40 m/s is the water hammer head generated at a time of 2L/a after the valve closure (Fig. 6). The water hammer head predicted by DVCM, DGCM, and GIVCM $H_{\max;v,1}$ = 210 m matches the measured head. Vaporous cavitation occurs in the pipeline (Fig. 7) following the formation of a vapor cavity at the valve (steep HGL slope). The duration of the first cavity at the valve $t_{\forall max;v,1}$ = [measurement: 0.318 (11.27L/a); DVCM: 0.307 (10.87L/a); DGCM: 0.310 (10.99L/a); GIVCM: 0.312 (11.05L/a)] s is much longer than the duration of the cavity for the experimental run with velocity 0.30 m/s. Only 18% of the negative water hammer head is reduced to reach the vapour pressure head at 2L/a. Head in the upstream end tank is relatively small compared with the water hammer head (12% for the 1.40-m/s case and 35% for the 0.30-m/s case). The head trace at the midpoint H_{mp} (Fig. 7) shows the existence of distributed vaporous cavitation regions, intermediate cavities, and shock waves. The shock waves gradually transform to water hammer waves before a large cavity collapses at the valve. The amount of released air is negligible because the wave induced by the cavity collapse at the valve propagates with a water hammer wave speed as a sharp

wavefront. It appears that higher-intensity cavitation along the pipeline blurs the short-duration pressure pulse after the first cavity collapses at the valve (Fig. 6); however, the magnitude of the pressure pulse incorporates the pulse due to cavity collapse and pulse reflected off the upstream end tank. Timing for the three numerical models is faster than for the experimental results, and this is more noticeable for DVCM results. In addition, DVCM exhibits a high-frequency pressure spike just prior to the collapse of the second cavity [Fig. 6(a)]. Again, the discrepancies between the numerical results are attributed to the different physical descriptions of vaporous cavitation and resulting phenomena along the pipeline. The maximum cavity volume at the valve for all three models is 4% of the reach volume; maximum cavity volumes along the pipeline are different. The order of magnitude of DVCM and DGCM cavity volumes at 15 interior computational sections is ~10–1,000 times smaller than the cavity volume at the valve. A small amount of gas in a cavity appears to give more realistic behavior. The GIVCM generates intermediate cavities at 12 interior sections during the transient event with about the same size of the cavity volume as for DVCM and DGCM. Shock celerities, as the shock moves into the vaporous zone, are 20–1,300 m/s. The ratio of the CPU user time for DVCM:DGCM:GIVCM is 1:1.6:5.

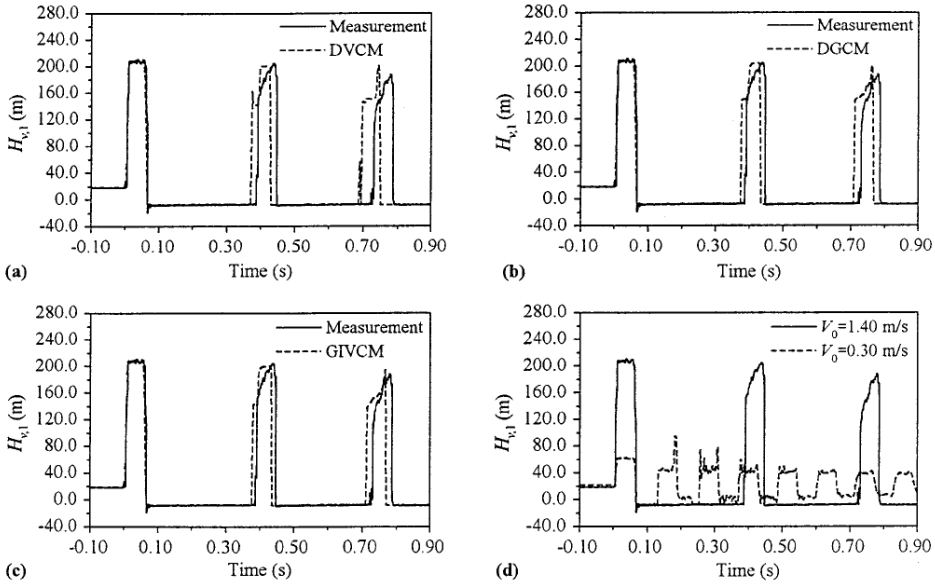

Fig 6: Comparison of Heads at Valve in Upward Sloping Pipe for DVCM, DGCM, GIVCM, and Measured Results; V_0 = 1.40 m/s

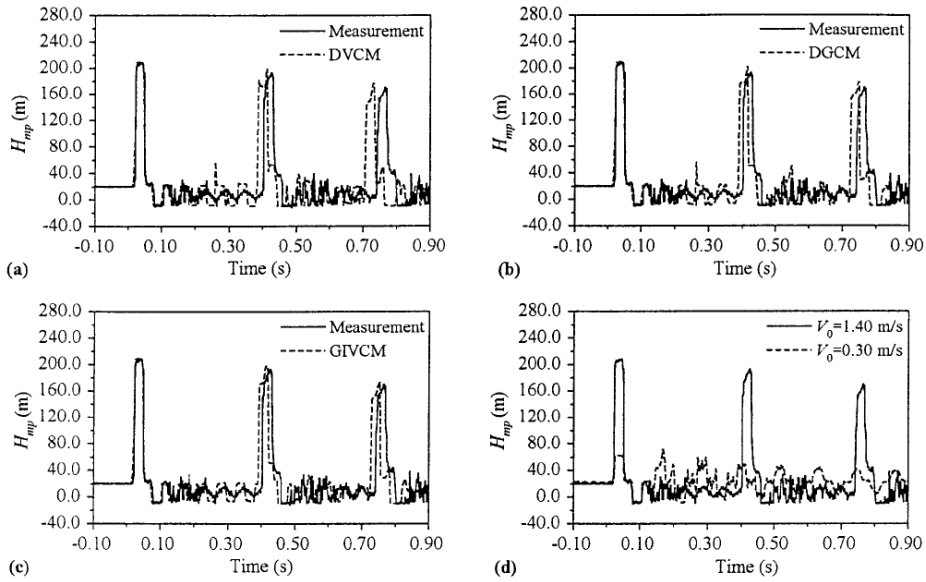

Fig 7: Comparison of Heads at Midpoint in Upward Sloping Pipe for DVCM, DGCM, GIVCM, and Measured Results; V_0 = 1.40 m/s

The upward sloping pipe allows (taking into account the initial flow conditions, pipe slope, and first cavity opening at the valve) the discrete cavity to be formed at the valve only (flat HGL) or discrete cavity at the valve and distributed vaporous cavitation region along the pipeline (steep HGL) (Simpson 1986; Bergant 1992).

Comparison of Numerical and Experimental Runs for Different Reservoir Static Heads

The results for two different static heads in the upstream end reservoir $H_{T,2}$ = (12.0; 22.0) m (Tank 2 in Fig. 2), and initial flow velocity V_0 = 0.30 m/s, are compared in Figs. 8 and 9. A valve closure for $H_{T,2}$ = 12.0 m generates column separation with a wide short-duration pressure pulse (Fig. 8) compared with $H_{T,2}$ = 22.0-m column separation with a narrow short-duration pressure pulse [Figs. 3–5 and 8(d)]. Again, the duration of the first cavity at the value is governed by the amount of valve closure head reduction to reach the vapour pressure head at $2L/a$ (60% of Joukowsky head ΔH for $H_{T,2}$ = 12.0 m compared with 76% of ΔH for $H_{T,2}$ = 22.0 m); the time of cavity existence at the value of $3.524L/a$ for $H_{T,2}$ = 12.0 m is correspondingly longer than $2.253L/a$ for $H_{T,2}$ = 22.0 m. Similarly, the magnitude and existence of the short-duration pressure pulse are dependent on the magnitude of the reservoir wave and relative timing of the cavity collapse at the valve and the reservoir wave reflection, respectively. The narrow pressure pulse occurs when the cavity at the valve collapses soon after the reflection of the reservoir wave off the cavity [Figs. 3–5 and 8(d)]; when the cavity at the valve collapses just prior to the reflection of the reservoir wave off the closed valve a wider pressure pulse occurs (Fig. 8) (Simpson 1986; Simpson and Wylie 1991; Bergant 1992). The decrease of static head at identical initial flow velocity results in a reduced amplitude of short-duration pressure pulse (lower amplitude reservoir wave) and more intense cavitation. All three numerical models accurately predict the magnitude of the wide short-duration pressure pulse and the duration of the first cavity at the valve in comparison with experimental results (Fig. 8).Timing for DVCM and DGCM is slightly slower for the third and fourth pressure pulses. The ratio of the CPU user time for DVCM:DGCM:GIVCM is 1:1.7:3.3.

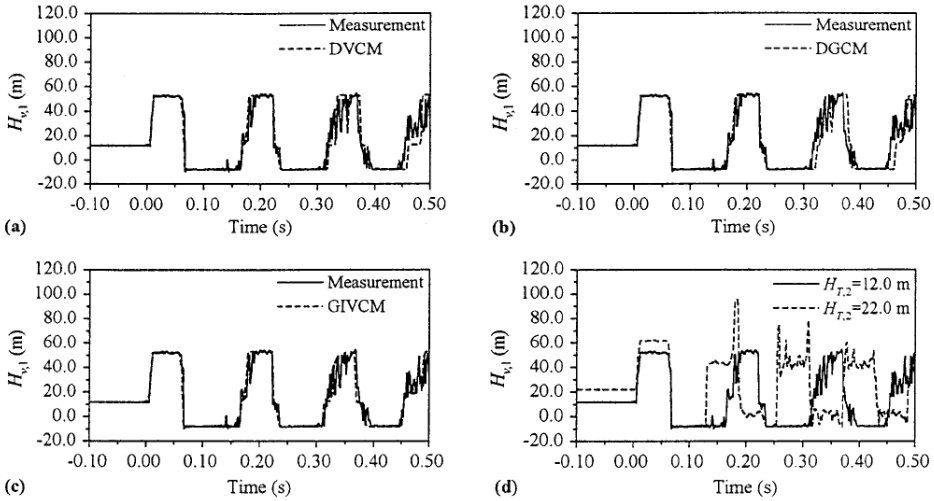

Fig 8: Comparison of Computed and Measured Heads at Valve in Upward Sloping Pipe for Different Static Heads; V_0 = 0.30 m/s

Comparison of Numerical and Experimental Runs for Different Pipe Slopes

The influence of pipe slope when comparing experimental runs for a downstream end valve closure in a downward ($\theta = -3.2°$) and an upward ($\theta = +3.2°$) sloping pipe (Fig. 2), for an identical initial flow velocity V_0 = 0.71 m/s and static pressure head at the valve of 20.0 m ($H_{T,1}$ = 20.0 m; $H_{T,2}$ = 22.0 m), is investigated. Computed and measured heads at the valve H_v and at the midpoint H_{mp} are shown in Figs. 10 and 11, respectively. The maximum computed heads in the downward sloping pipe $H_{\max;v,2}$ = (DVCM: 115.3; DGCM: 117.0; GIVCM: 115.3) m are slightly lower than the maximum measured head $H_{\max;v,2}$ = 122.1 m. The maximum head for DGCM and measurement occurs after the first cavity collapse; whereas the valve closure head is the maximum head for DVCM and GIVCM. The maximum computed and measured head in the upward sloping pipe $H_{\max;v,1}$ = 117.4 m is the water

hammer head. The duration of the first cavity at the valve in the downward sloping pipe $t_{\forall max;v,1}$ = [measurement: 0.1626 (5.761L/a); DVCM, DGCM, GIVCM: 0.1622 (5.745L/a)] s is slightly shorter than in the upward sloping $t_{\forall max;v,1}$ = [measurement: 1 0.1668 (5.910L/a); DVCM, DGCM, GIVCM: 0.1657 (5.870L/a)] s. The slightly different timing of the cavity collapse at the valve (Fig. 10) and intensity of cavitation along the pipeline (Fig. 11) are caused by the difference in head envelope (hydraulic grade line) and pipe slope (profile), and the direction of the action of gravity. The gravity force is acting in the positive direction in the downward sloping pipe and in the negative direction in the upward sloping pipe relative to the position of the valve with a large cavity. More intense cavitation along the pipe in the downward sloping pipe (Fig. 11) blurs the short-duration pressure pulse at the valve (Fig. 10). The pressure pulse in the upward sloping pipe resembles the wide short-duration pressure pipe. In addition, the downward sloping pipe allows a distributed vaporous cavitation region and intermediate cavities to form along the pipe prior to the discrete cavity opening at the valve. The three numerical models do not predict some of the high-frequency, low-amplitude pressure spikes found by measurements. The ratio of CPU user time for the downward sloping pipe run for DVCM, DGCM, GIVCM is 1:1.7:3.7, and for the upward sloping run it is 1:1.7:2.5.

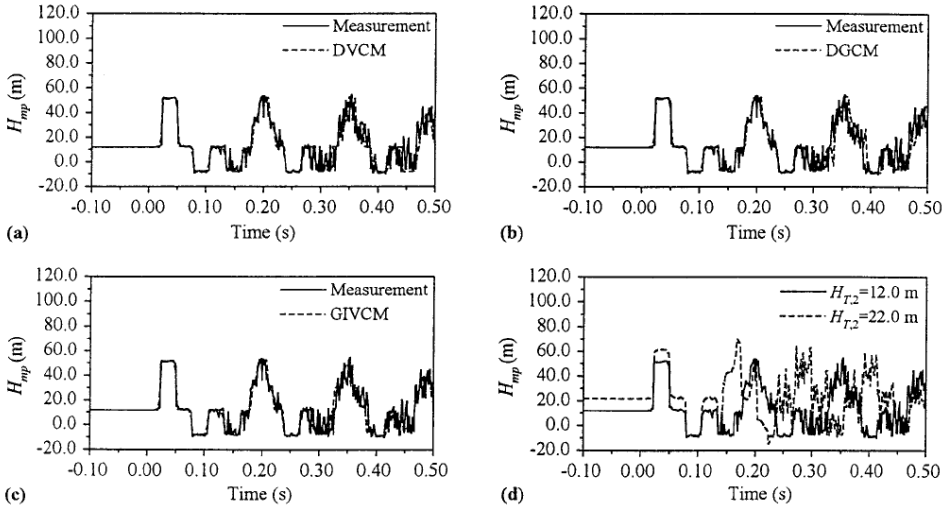

Fig 9: Comparison of Computed and Measured Heads at Midpoint in Upward Sloping Pipe for Different Static Heads; V_0 = 0.30 m/s

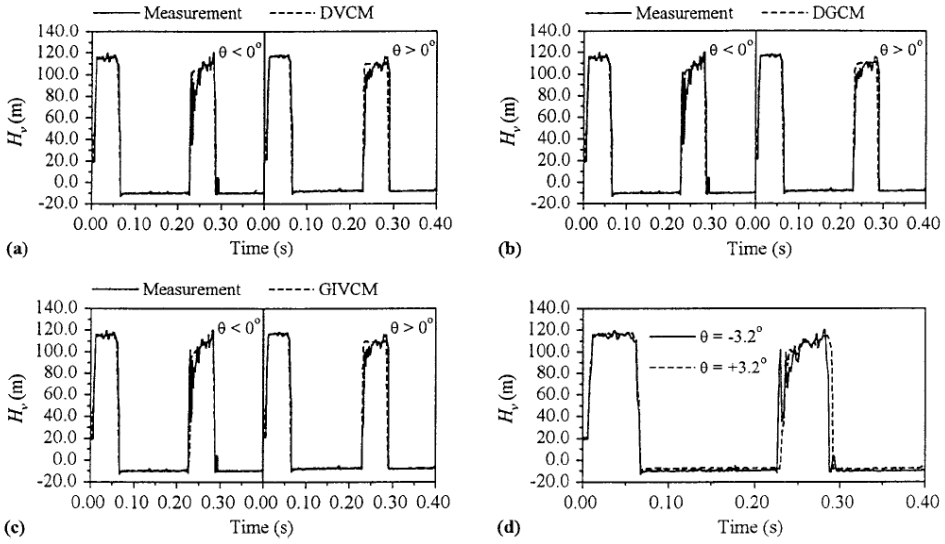

Fig 10: Comparison of Computed and Measured Heads at Valve in Upward and Downward Sloping Pipe; V_0 = 0.71 m/s

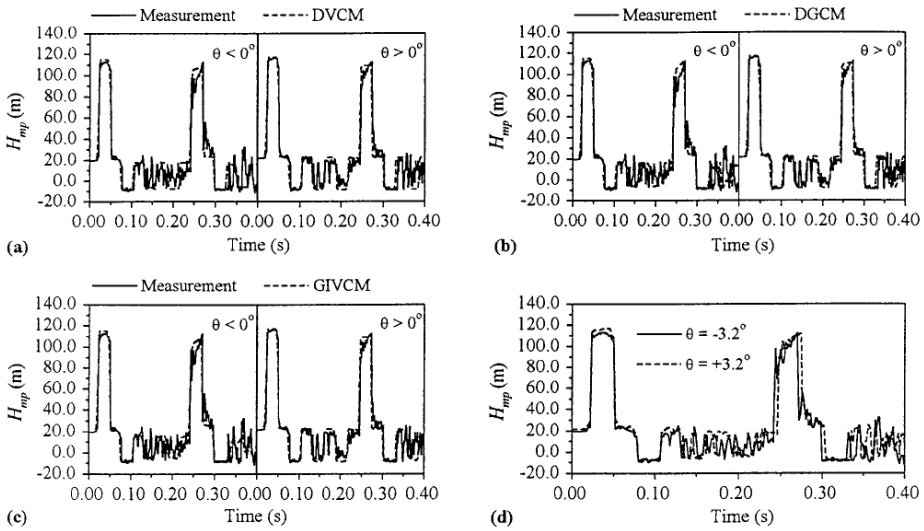

Fig 11: Comparison of Computed and Measured Heads at Midpoint in Upward and Downward Sloping Pipe; V_0 = 0.71 m/s

Global Comparison of Numerical and Experimental Results

The results of computations and measurements are compared for a number of flow regimes initiated by a rapid closure of the valve in a downward and an upward sloping pipe (Fig. 2). A comparison is made for 15 initial velocities V_0 = (0.10– 1.50; velocity increment 0.10 $\pm$ 0.02) m/s at two identical static heads at the valve of 10.0 and 20.0 m [$H_{T,1}$ = (10.0; 20.0) m for θ = 23.2°; $H_{T,2}$ = (12.0; 22.0) m for θ = 13.2°]. The objective of the analysis is to verify the performance of the three column separation models (DVCM, DGCM, and GIVCM) for a broad range of parameters (robustness of the models).

A comparison is made for the ratio of maximum head rise at the valve $(H_{max} - H_0)_v$ to the Joukowsky head rise aV_0/g (Fig. 12) in which H_0 = steady-state head at the valve. A pipeline must be designed to withstand the maximum and minimum pressure (vapor pressure for column separation case). Fig. 12 shows that all three models give accurate maximum pressure for velocity cases with a maximum head rise equal or slightly higher than the Joukowsky head rise. The discrepancies between computed and measured results increase for velocity cases generating narrow short-duration pressure pulses. The occurrence of narrow short-duration pressure pulses may be observed from Fig. 13, showing the duration of the maximum cavity volume at the valve $t_{\forall max;v,1}$ (first cavity) to the reflection time L/a (also see Figs. 3, 4, or 5). A narrow short-duration pressure pulse occurs for $t_{\forall max;v,1}$ slightly higher than an exact multiple of $2L/a$. The GIVCM gives slightly better results than DVCM and DGCM for these cases. There is reasonable agreement between the computed and measured $t_{\forall max;v,1}$ for all three models and velocity cases (Fig. 13). The maximum cavity volume at the valve of 6.2% of the reach volume occurs for the case with V_0 = 1.50 m/s, $H_{T,2}$ = 12.0 m, and θ = 13.2°.

The discrepancies between the measured and computed results found by temporal and global comparisons may be attributed to approximate modeling of column separation along the pipeline (distributed vaporous cavitation region, actual number, and position of intermediate cavities), resulting in slightly different timing of the cavity collapse and superposition of the waves (Bergant 1992; Simpson and Bergant 1994). In addition, discrepancies may also originate from discretization in the numerical models [$\Delta t = L/(aN) = 37.23/(1319 \times 16) = 0.00176$ s], the unsteady friction term being approximated as a steady-state friction term and uncertainties in measurement (Simpson and Bergant 1996).

Classification of Column Separation Flow Regimes

A parametric numerical analysis has been performed to compute critical flow conditions and to predict column separation flow regimes for a broad range of parameters including the flow velocity and static upstream tank head in the upward and downward sloping pipes (Fig. 2). The numerical

analysis is carried out using the DGCM. Transient regimes in the upward and the downward sloping pipe for a rapid closure of the downstream end valve were investigated for 151 initial flow velocities V_0 = (0.05–1.55, velocity increment 0.01) m/s and 5 static heads in the upstream end tank H_T = [5.0, 10.0, 15.0, 20.0, 25.0 for θ = 23.2°; and 7.0, 12.0, 17.0, 22.0, 27.0 for θ = 13.2° (Fig. 2)]. The parameters selected for each computational run are identical to parameters selected for the model and measurement comparison analysis (valve closure time t_c = 0.009 s, wave speed a = 1319 m/s, number of reaches N = 16, gas void fraction $\alpha_g = 10^{-7}$, and weighting factor ψ = 1.0).

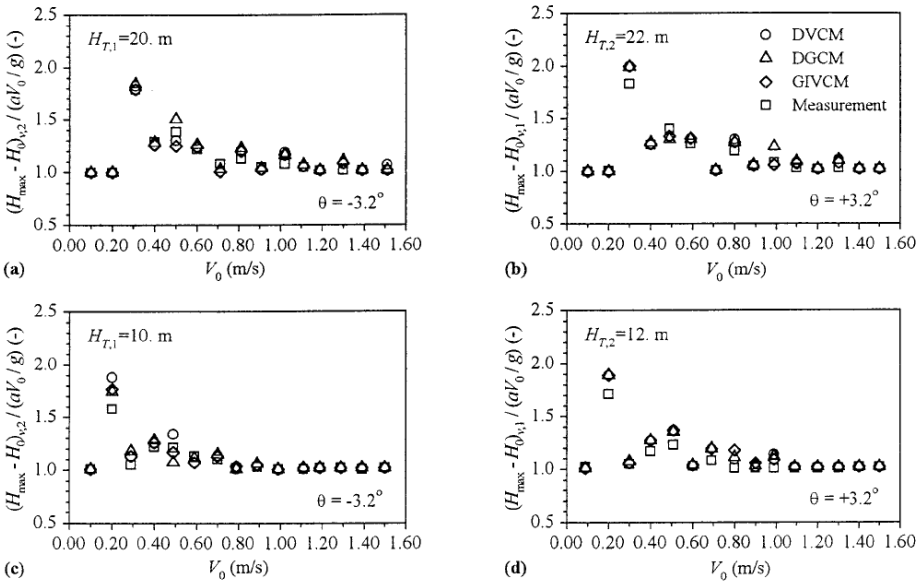

Fig 12: Comparison of Maximum Head at Valve for Computed and Measured Results

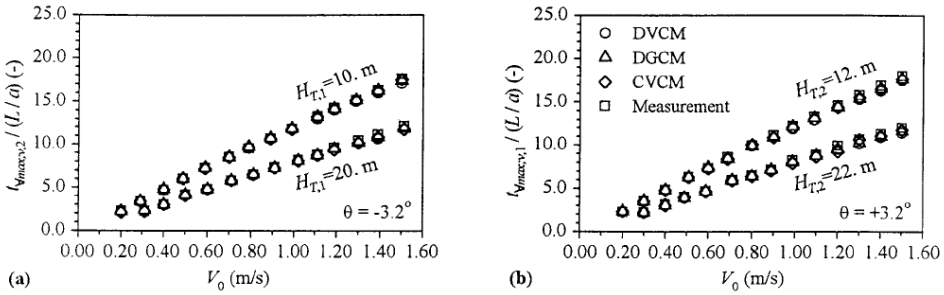

Fig 13: Comparison of Duration of Maximum Cavity Volume at Valve for Computed and Measured Results

Numerical results are presented for the maximum piezometric head at the valve $H_{max;v}$ [Figs. 14(a) and 14(b)] and for the ratio of maximum pressure head rise $(H_{max} - H_0)_v$ to the Joukowsky pressure head rise aV_0/g [Figs. 14(c) and 14(d)]. $H_{max;v}$ is the maximum head in the pipeline during water hammer and column separation events.

Numerical results clearly show the influence of the initial velocity, static upstream tank head, and pipe slope on the maximum head at the valve as found by the model and measurement comparison analysis. Water hammer with no column separation occurs for low-flow velocities. Column separation starts at velocities V_0 higher than (0.10, 0.13, 0.18, 0.21, 0.25) m/s for respective reservoir heads $H_{T,1}$ = (5.0, 10.0, 15.0, 20.0, 25.0) m in a downward sloping pipe (θ = 23.2°) and V_0 higher than (0.11, 0.15, 0.18, 0.22, 0.26) m/s for respective $H_{T,2}$ = (7.0, 12.0, 17.0, 22.0, 27.0) m in an upward sloping pipe (θ = 13.2°). Short-duration pressure pulses may be identified as ‘‘triangular waves’’ in Fig. 14 with a period of $2L/a$ superimposed on the water hammer head line. The upper bound of the triangular wave captures the narrow-type short-duration pressure pulses, whereas the lower band encompasses wide short-duration pressure pulses. Attenuation of the wave is related to the magnitude of the upper

reservoir wave (shock, water hammer) and the intensity of cavitation along the pipeline. The maximum head for higher velocity column separation cases gradually attenuates to the water hammer head. For the lower three upstream tank static head levels, the maximum head remains as the water hammer head for velocities V_0 higher than (0.92, 1.21, 1.50) m/s in a downward sloping pipe, and for V_0 higher than (1.02, 1.20, 1.51) m/s in an upward sloping pipe. The parametric analysis shows stronger attenuation of short-duration pressure pulses in a downward sloping pipe that may have contributed to more intense cavitation along the pipe. In addition, the triangular waves indicate the potential magnitude of discrepancies between computed and measured maximum heads.

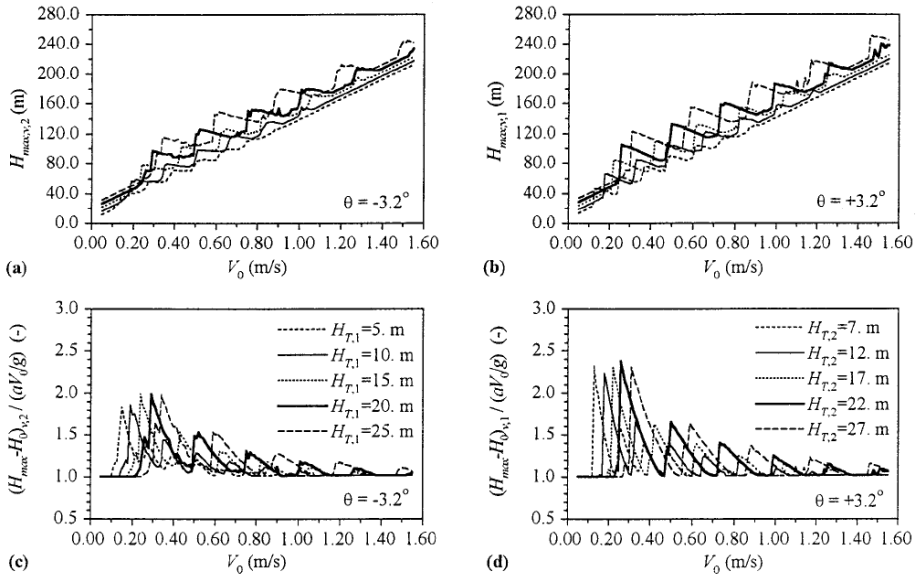

Fig 14: Computed Maximum Head at Valve

Transient regimes investigated experimentally and theoretically in a simple reservoir-pipeline-valve system (Fig. 2) may be classified regarding the physical state of the liquid and the maximum pipeline pressure as follows:

1. Water hammer flow regime: No column separation occurs during transients.
2. Active column separation flow regime: The maximum pipeline pressure is generated following the column separation at the valve and along the pipeline (active column separation from the designer's point of view). The maximum pressure at the valve is governed by the intensity of the short-duration pressure pulse (region of triangular waves in Fig. 14).
3. Passive column separation flow regime: The maximum pipeline pressure is the water hammer pressure before intense cavitation occurs.

CONCLUSIONS

This paper considers the interaction between vapor cavity collapse, the presence of vaporous cavitation, and the occurrence of high pressures in the form of short-duration pressure pulses following column separation in pipelines. A generalized set of column separation equations for pipelines has been presented. Numerical schemes for the solution of these equations are described and three column separation models including the DVCM, DGCM, and GIVCM are presented. The DVCM and DGCM involve a relatively simple numerical algorithm in comparison with the GIVCM. However, the GIVCM enables direct tracking of actual column separation phenomena (e.g., discrete cavities, vaporous cavitation zones), and consequently, better insight into the transient event. A comparison for a number of results from the three numerical column separation models and experimental results for a sloping pipe laboratory apparatus are given. The principle source of discrepancies between the computed and measured column separation results appears to originate from the method of physical description of vaporous cavitation and resulting phenomena along the pipeline. The discrete gas cavity model has been used to characterize column separation regimes

found by experiments for both an upward and downward sloping pipe resulting from the rapid closure of a valve. An approach has been developed in this paper to identify column separation modes for a broad range of parameters including initial flow velocity, static head, and pipe slope. Active column separation has been used to define situations where the collapse of a vapor cavity results in a maximum pressure or short-duration pressure pulse that exceeds the Joukowsky pressure rise for a rapid valve closure.

ACKNOWLEDGMENTS

The support of the Slovenian Ministry of Science and Technology, Slovenian Science Foundation, Litostroj E.I. of Slovenia, and the Australian Research Council are gratefully acknowledged. The thoughtful comments of the reviewers were very much appreciated, the incorporation of their comments has improved the paper significantly.

APPENDIX I. REFERENCES

Almeida, A. B. (1992). ''Accidents and incidents: A harmful/powerful way to develop expertise on pressure transients.'' *Hydraulic transients with water column separation*, E. Cabrera and M. A. Fanelli, eds., Fluid Mechanics Group, Universidad Politechnica de Valencia, Valencia, Spain, 379–400.

Anderson, A., and Arfaie, M. (1992). ''Variable water hammer wave speed in column separation.'' *Hydraulic transients with water column separation*, E. Cabrera and M. A. Fanelli, eds., Fluid Mechanics Group, Universidad Politechnica de Valencia, Valencia, Spain, 183–199.

Anderson, A., Arfaie, M., Sandoval-Pena, R., and Suwan, K. (1992). ''Column separation behaviour modes in a simple test rig.'' *Hydraulic transients with water column separation*, E. Cabrera and M. A. Fanelli, eds., Fluid Mechanics Group, Universidad Politechnica de Valencia, Valencia, Spain, 33–47.

Barbero, G., and Ciaponi, C. (1992). ''Experimental validation of a discrete free gas model for numerical simulation of hydraulic transients with cavitation.'' *Hydraulic transients with water column separation*, E. Cabrera and M. A. Fanelli, eds., Fluid Mechanics Group, Universidad Politechnica de Valencia, Valencia, Spain, 51–67.

Bergant, A. (1992). ''Transient cavitating flow in pipelines,'' PhD thesis, University of Ljubljana, Ljubljana, Slovenia (in Slovene).

Bergant, A., and Simpson, A. R. (1992). ''Interface model for transient cavitating flow in pipelines.'' *Unsteady flow and fluid transients*, R. Bettess and J. Watts, eds., Balkema, Rotterdam, The Netherlands, 333– 342.

Bergant, A., and Simpson, A. R. (1994). ''Estimating unsteady friction in transient cavitating pipe flow.'' *Water pipeline systems*, D. S. Miller, ed., Mechanical Engineering Publications, London, 3–16.

Bergant, A., and Simpson, A. R. (1995). ''Water hammer and column separation measurements in an experimental apparatus.'' *Res. Rep. No. R128*, Dept. of Civ. and Envir. Engrg., The University of Adelaide, Adelaide, Australia.

Bergant, A., and Simpson, A. R. (1996). ''Visualisation of transient cavitating flow in pipelines.'' *Strojniski vestnik—J. Mech. Engrg.*, Ljubljana, Slovenia, 42(1–2), 1–16.

Bonin, C. C. (1960). ''Water-hammer damage to Oigawa Power Station.'' *J. Engrg. for Power*, 82(2), 111–119.

Brunone, B., and Greco, M. (1990). ''Un modello per la riconstruzione di fenomeni di colpo d'ariete anche in prezenca di cavitazione.'' *Proc., 22nd Italian Congr. of Hydr. and Hydr. Constr.*, 4, 147–160 (in Italian).

Carmona, R., Sanchez, J. L., and Carmona, L. (1988). ''A simplified procedure to evaluate liquid column separation phenomena.'' *Water Power & Dam Constr.*, London, 40(12), 42–46.

Carnahan, B., Luther, H. A., and Wilkes, J. O. (1969). *Applied numerical methods*. Wiley, New York.

Coleman, H. W., and Steele, W. G. (1989). *Experimentation and uncertainty analysis for engineers*. Wiley, New York.

Fan, D., and Tijsseling, A. (1992). ''Fluid-structure interaction with cavitation in transient pipe flows.'' *J. Fluids Engrg.*, 114(2), 268–274.

Hansson, I., Kerdinskii, V., and Morch, K. A. (1982). ‘‘On the dynamics of cavity clusters.’’ *J. Phys. D: Appl. Phys.*, 15(9), 1725–1734.
Joukowsky, N. (1900). ‘‘U¨ ber den hydraulischen Stoss in Wasserleitungen.’’ *Memoirs de l’academie imperiale de St.-Petersbourg. Classe physico-mathematique*, St. Petersburg, Russia, 9(5) (in German).
Kot, C. A., and Youngdahl, C. K. (1978). ‘‘Transient cavitating effects in fluid piping systems.’’ *Nuclear Engrg. and Design*, Amsterdam, The Netherlands, 45(1), 93–100.
Martin, C. S. (1983). ‘‘Experimental investigation of column separation with rapid closure of downstream valve.’’ *Proc., 4th Conf. on Pressure Surges*, British Hydromechanics Research Association, Cranfield, U.K., 77–88.
Miwa, T., Sano, M., and Yamamoto, K. (1990). ‘‘Experimental studies on water hammer phenomenon including vapour column separation.’’ *Water Supply*, Oxford, England, U.K., 8(3–4), 430–438.
Parmakian, J. (1985). ‘‘Water column separation in power and pumping plants.’’ *Hydro Review*, Summer, 85–89.
Provoost, G. A. (1976). ‘‘Investigations into cavitation in a prototype pipeline caused by water hammer.’’ *Proc., 4th Conf. on Pressure Surges*, British Hydromechanics Research Association, Cranfield, England, U.K., 77–88.
Provoost, G. A., and Wylie, E. B. (1981). ‘‘Discrete gas model to represent distributed free gas in liquids.’’ *Proc., 5th Int. Symp. on Column Separation*, International Association for Hydraulic Research, Delft, The Netherlands, 249–258.
Safwat, H. H., Aratsu, A. H., and Husaini, S. H. (1986). ‘‘Generalized applications of the method of characteristics for the analysis of hydraulic transients involving empty sections.’’ *Proc., 5th Conf. on Pressure Surges*, British Hydromechanics Research Association, Cranfield, U.K., 157–167.
Safwat, H. H., and van der Polder, J. (1973). ‘‘Experimental and analytic data correlation study of water column separation.’’ *J. Fluids Engrg.*, 94(1), 91–97.
Simpson, A. R. (1986). ‘‘Large water hammer pressures due to column separation in a sloping pipe,’’ PhD thesis, University of Michigan, Ann Arbor, Mich.
Simpson, A. R., and Bergant, A. (1994). ‘‘Numerical comparison of pipe column-separation models.’’ *J. Hydr. Engrg.*, ASCE, 120(3), 361–377.
Simpson, A. R., and Bergant, A. (1996). ‘‘Interesting lessons from column separation experiments.’’ *Pressure surges and fluid transients in pipelines and open channels*, A. Boldy, ed., Mechanical Engineering Publications Ltd., Bury St. Edmunds, U.K., 83–97.
Simpson, A. R., and Wylie, E. B. (1991). ‘‘Large water hammer pressures due to column separation in pipelines.’’ *J. Hydr. Engrg.*, ASCE, 117(10), 1310–1316.
Streeter, V. L. (1969). ‘‘Water hammer analysis.’’ *J. Hydr. Div.*, ASCE, 95(6), 1959–1972.
Streeter, V. L. (1983). ‘‘Transient cavitating pipe flow.’’ *J. Hydr. Engrg.*, ASCE, 109(11), 1408–1423.
Wylie, E. B. (1984). ‘‘Simulation of vaporous and gaseous cavitation.’’ *J. Fluids Engrg.*, 106(3), 307–311.
Wylie, E. B., and Streeter, V. L. (1993). *Fluid transients in systems*. Prentice- Hall, Englewood Cliffs, N.J.

APPENDIX II. NOTATION

The following symbols are used in this paper:

A = pipe area;
A_m = pipe area in distributed vaporous cavitation region;
a = water hammer wave speed;
a_s = shock wave speed;
B_M, B = known constants in water hammer compatibility equations;
C_M, C_P = known constants in water hammer compatibility equations;
D = pipe diameter;
f = Darcy-Weisbach friction factor;
f_s = sampling frequency;
g = gravitational acceleration;
H = piezometric head (head, hydraulic grade line);
$H_{\max;v}$ = maximum piezometric head at valve;

H_{mp} = piezometric head at midpoint;
H_q = piezometric head at quarter point;
H_s = piezometric head on water hammer side of shock wave front;
H_{sv} = piezometric head on distributed vaporous cavitation side of shock wave front;
H_T = piezometric head in reservoir;
H_v = piezometric head at valve;
H_0 = steady-state head;
L = pipe length; length of liquid plug;
N = number of reaches in pipeline;
p = pressure
p_R = regulated air pressure;
p_s = pressure on water hammer side of shock wave front;
p_{sv} = pressure on distributed vaporous cavitation side of shock wave front;
p_T = tank pressure;
Q = discharge or discharge at downstream side of computational section;
Q_u = discharge at upstream side of computational section;
T = temperature;
t = time;
t_c = valve closure time;
t_i = time of cavitation inception;
t_{in} = time of inception of discrete vapor cavity;
t_r = time of flow reversal in liquid-vapor mixture zone;
$t_{\forall max;v}$ = duration of first cavity at valve;
U_x = uncertainty in measurement;
V = flow velocity or velocity at downstream side of vapour cavity;
V_m = liquid-vapor mixture velocity;
V_{mi} = inception velocity of liquid-vapor mixture;
V_{mt} = terminal velocity in the distributed cavitation region;
V_u = velocity at upstream side of vapor cavity;
V_0 = initial flow velocity;
X = distance;
α = valve opening;
α_g = gas void fraction;
α_v = void fraction of vapor;
ΔH = Joukowsky pressure head rise;
Δt = time step;
Δx = reach length;
Δx = control volume length;
θ = pipe slope;
ρ = liquid density;
ρ_m = liquid-vapor mixture density;
ψ = weighting factor; and
$\forall_{vc}$ = discrete vapor cavity volume.

Subscripts

g = gas;
j = computational section index;
k = reach index;
m = liquid-vapor mixture;
mi = condition of inception of vaporous cavitation;
mt = terminal velocity in liquid-vaporous mixture zone;
s = shock wave front;
u = upstream;
v = vapor; and
vc = discrete vapor cavity.